ORIGINAL ARTICLE

Coda wave attenuation in the Parecis Basin, Amazon Craton, Brazil: sensitivity to basement depth

**Lucas Vieira Barros · Marcelo Assumpção ·
Ronnie Quintero · Vinicius Martins Ferreira**

Abstract Small local earthquakes from two after-shock sequences in Porto dos Gaúchos, Amazon craton—Brazil, were used to estimate the coda wave attenuation in the frequency band of 1 to 24 Hz. The time-domain coda-decay method of a single backscattering model is employed to estimate frequency dependence of the quality factor (Q_c) of coda waves modeled using $Q_c = Q_0 f^\eta$, where Q_0 is the coda quality factor at frequency of 1 Hz and η is the frequency parameter. We also used the independent frequency model approach (Morozov, Geophys J Int, 175:239–252, 2008), based in the temporal attenuation coefficient, $\chi(f)$ instead of $Q(f)$, given by the equation $\chi(f) = \gamma + \frac{\pi f}{Q_e}$, for the calculation of the geomet-rical attenuation (γ) and effective attenuation (Q_e^{-1}). Q_c values have been computed at central frequencies (and band) of 1.5 (1–2), 3.0 (2–4), 6.0 (4–8), 9.0 (6–12), 12 (8–16), and 18 (12–24) Hz for five different datasets selected according to the geotectonic environment as well as the ability to sample shallow or deeper structures, particularly the sediments of the Parecis basin and the crystalline basement of the Amazon craton. For the Parecis basin $Q_c = (98 \pm 12) f^{(1.14\pm0.08)}$, for the surrounding shield $Q_c = (167 \pm 46) f^{(1.03\pm0.04)}$, and for the whole region of Porto dos Gaú-chos $Q_c = (99 \pm 19) f^{(1.17\pm0.02)}$. Using the inde-pendent frequency model, we found: for the cra-tonic zone, $\gamma = 0.014$ s^{-1}, $Q_e^{-1} = 0.0001$, $\nu \approx 1.12$; for the basin zone with sediments of $\sim$500 m, $\gamma = 0.031$ s^{-1}, $Q_e^{-1} = 0.0003$, $\nu \approx 1.27$; and for the Parecis basin with sediments of $\sim$1,000 m, $\gamma = 0.047$ s^{-1}, $Q_e^{-1} = 0.0005$, $\nu \approx 1.42$. Analysis of the attenuation factor (Q_c) for different values of the geometrical spreading parameter (ν) indicated that an increase of ν generally causes an increase in Q_c, both in the basin as well as in the craton. But the differences in the attenuation between different geological environments are maintained for different models of geometrical spreading. It was shown that the energy of coda waves is atten-uated more strongly in the sediments, $Q_c = (78 \pm 23) f^{(1.17\pm0.14)}$ (in the deepest part of the basin), than in the basement, $Q_c = (167 \pm 46) f^{(1.03\pm0.04)}$ (in the craton). Thus, the coda wave analysis can

L. Vieira Barros (✉) · V. M. Ferreira
Observatório Sismológico, Universidade de Brasília,
70910-900 Brasília, DF, Brazil
e-mail: lucas@unb.br

V. M. Ferreira
e-mail: vinicius2002@gmail.com

M. Assumpção
IAG, Universidade de São Paulo, 05508-090,
São Paulo, SP, Brazil
e-mail: marcelo@iag.usp.br

R. Quintero
OVSICORI-UNA, Universidad Nacional
de Costa Rica, Heredia, Costa Rica
e-mail: rquinter@una.ac.cr

contribute to studies of geological structures in the upper crust, as the average coda quality factor is dependent on the thickness of sedimentary layer.

Keywords Amazon craton—Brazil · Coda wave attenuation · Porto dos Gaúchos seismic zone

1 Introduction

Seismic attenuation plays an important role in studies of the earth structure, from which useful information on medium properties can be inferred. Determination of source parameters must take into account the proper attenuation characteristic of the wave path. Moreover, it is essential for seismic risk studies and seismic hazard assessment, and consequently for seismic risk mitigation. In the last three decades, different studies in many parts of the world have used coda waves from small earthquakes to determine local attenuation properties of the crust (Dias and Souza 2004; Gupta et al. 1995; Herrmann 1980; Ibáñez et al. 1990; Pulli 1984; Singh and Herrmann 1983).

Coda waves from small local earthquakes are the superposition of backscattered body waves generated from numerous heterogeneities distributed randomly in the lithosphere (Aki 1969; Aki and Chouet 1975; Rautian and Khalturin 1978). Therefore, the great variety of paths traveled by these scattered waves provides information concerning the average attenuation properties of the medium instead of just the characteristics of a particular path (Gupta et al. 1995). The attenuation of the seismic waves in the lithosphere is highly frequency dependent and is caused by the combination of two effects: scattering and anelastic attenuation (Havskov et al. 1989) and it is difficult to separate each other, since both have similar dependence on travel time or distance (Aki 1969; Havskov et al. 1989). Anelastic attenuation is strongly dependent on the tectonic environment, as demonstrated in many studies carried out in different places of the world (e.g., Havskov et al. 1989).

One factor that increases seismic hazard in intraplate regions is the low attenuation of seismic waves, which travel in more homogeneous medium than those of interplate regions. Thus, de-spite the low seismic activity in stable continental regions, the level of ground shaking caused by a moderate intraplate earthquake reaches a larger area compared to similar magnitudes in plate border areas (Nuttli 1973). Moreover, because of the low seismicity, studies of seismic wave attenuation in stable continental interiors are rare, particularly in Brazil, due to poor coverage of seismic stations. In Brazil, only Dias and Souza (2004) and Carvalho and Souza (2006) have estimated coda Q attenuation. They studied the seismogenic João Câmara area in NE Brazil, and suggested that the seismogenic fault is a boundary between two different seismic attenuation zones. Additionally, Souza and Mitchell (1998) have studied Lg coda Q attenuation in most of South America.

Porto dos Gaúchos seismic zone (PGSZ) is among the most seismically active in Brazil. Three of the 14 largest intraplate earthquakes (magnitudes ≥ 5.0 m_b) reported in the Brazilian continental lithosphere occurred in PGSZ. This includes the largest earthquake in the stable continental interior of the South American plate, which occurred on January 31, 1955, with 6.2 m_b and VIII-IX inferred MM intensity, shown by the large star in Fig. 1 (Barros et al. 2009; Johnston 1989). The other two occurred on March 10, 1998 (5.2 m_b, MMI VI) and on March 23, 2005 (5.0 m_b, MMI V) in the same seismic zone (shown by the small star in Fig. 1) 100 km NE of the 1955 epicenter. In this area a recurrent seismic activity has been observed since 1959, with several earthquakes occurring in subsequent years (Barros et al. 2009).

The economic development of this region in the last three decades has increased the importance of seismic risk studies for this area. Estimates of attenuation coefficients are important for seismic hazard assessment. This attenuation study aims to contribute to future seismic source studies and to mitigate seismic risk in the region.

Many measurements of coda Q in the world have been carried out in different tectonic and geological settings. Partial compilations of Q_0 and η (e.g., Jin and Aki 1988; Morozov 2008; Sharma et al. 2007) have indicated a trend of higher Q_0 (roughly 100 to 1,000) and lower η (about 0.3 to 0.7) for stable continental regions compared with tectonically active areas ($Q_0 = 40$–200, $\eta = 0.7$ to 1.1). However, a large overlap exists in coda Q

results for these two environments, especially in the $Q_0 = 100–200$ range. Part of this scatter could be due to different surface geology (predominance of sedimentary or igneous rocks). The results for the intraplate PGSZ presented here will contribute to the studies of possible systematic differences in attenuation properties between tectonically active and stable areas.

In the present paper, the single scattering model and the independent frequency model approach or f model (Morozov 2008, 2009a, b, Morozov et al. 2008) are used to study the coda Q attenuation in Porto dos Gaúchos Seismic Zone, located in the Parecis basin, Amazon craton, Brazil.

2 Tectonic setting and seismicity of the study area

The PGSZ is located in the center north of Mato Grosso State, in the contact between the southern part of the Amazonian craton and the northern part of the Phanerozoic Parecis basin (Fig. 1).

The study area (Fig. 2) includes the Precambrian basement of the Amazon craton, composed mainly by granitic/gneissic rocks, and Phanerozoic terrains with sedimentary rocks of the Parecis basin. The Precambrian basement of the Amazon craton belongs to the Rio Negro-Juruena geochronologic province with 1.8 to 1.55 Ga (Tassinari et al. 2000), with an important feature, the Caiabis graben of Mesoproterozoic age (~1.36 Ga, Leite and Saes 2003, as shown in Fig. 1). For simplicity, we will call the area outside the basin as "craton".

The main trend of the gravity anomalies near the PGSZ is oriented in the NW-SE direction related to the Brasnorte gravity high (Fig. 1). However, the epicentral distribution of the recent (1998 to 2005) seismicity correlates better with a series of ENE-WSW aeromagnetic lineaments near PGSZ which probably indicate major
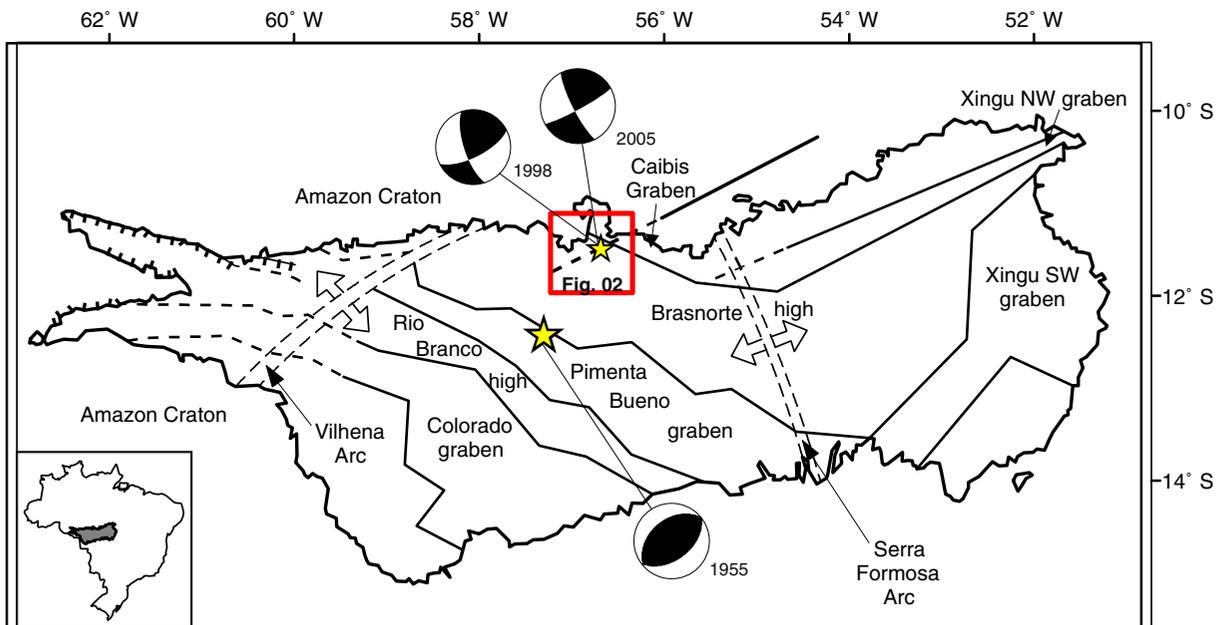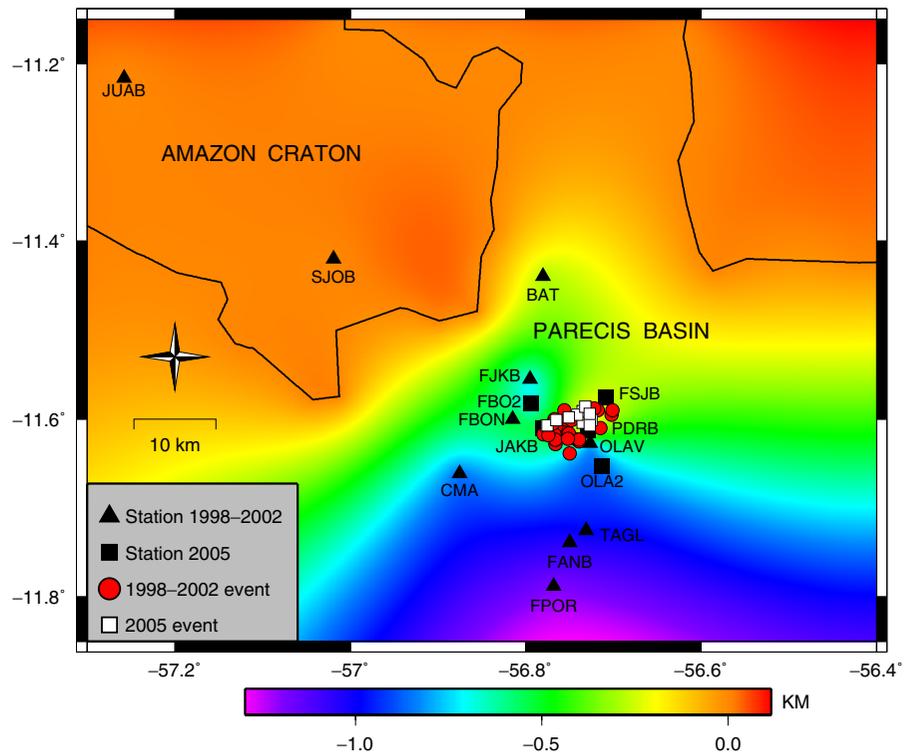

Fig. 1 Simplified tectonic domains of the Parecis basin (modified from Bahia et al. 2007) with the sequence of WNW-ESE trending grabens and basement highs. The *thick solid line* (N 60° E) in the Caiabis graben is the WSW-ENE fault from Leite and Saes (2003), extrapolated with *dashed line* towards the 1998/2005 epicentral area. The *red square* indicates the study area shown in Fig. 2. The *stars* indicate the epicenters of 1998/2005 and 1955 earthquakes, and the *beach balls* are the focal mechanism solutions for the 1955 (Mendiguren and Richter 1978) and 1998/2005 earthquakes (Barros et al. 2009)

basement faulting during the geological evolution of this area (Barros et al. 2009).

In Porto dos Gaúchos, a recurrent seismicity has been observed since 1959 (MM intensity IV–V), 2 years after the arrival of the first settlements in that remote area of the Amazon forest. Since 1980, with the installation of regional stations in the Amazon, seven events with magnitudes between 3.5 and 4.4 have been detected. On March 10, 1998, a 5.2 m_b and MMI VI was detected. A local seismic network was deployed by the University of Brasília to study the aftershock activity (Fig. 2). This network, with up to seven 3-component stations, detected more than 2,500 events by December 2002, when it was deactivated.

On March 23, 2005, another shock occurred in PGSZ, with magnitude 5.0 m_b and intensity V (MM). One week later, five stations were installed to monitor the aftershocks. This time the stations could be installed closer to the known epicentral area. In 3 months, this network detected more than 3,500 micro-earthquakes. Hypocenters were

located with a velocity model derived from a seismic refraction experiment (Barros et al. 2009).

Focal mechanism studies of the 1955 earthquake by Mendiguren and Richter (1978) indicated a pure reverse faulting with P axis oriented roughly in SE-NW direction. Both the 1998 and 2005 earthquakes sequences occurred in a single WSW–ENE oriented fault zone with right-lateral strike-slip mechanisms suggesting compressional SHmax roughly in the E-W direction (Barros et al. 2009; Fig. 1). The epicentral zone for both the 1998–2002 (hereafter 1998 sequence) and 2005 sequences (about 6 km long) are indicated by circles and squares in Fig. 2. This figure shows the basement depth in the Parecis basin as obtained by Barros and Assumpção (2009) using Receiver Function techniques applied to local events. It can be seen that the seismicity occurs in a basement high (PDRB station is located on an isolated granite outcrop within the basin). The sediment thickness increases from north to south up to about 1,400 m depth beneath FPOR station. The stations CMA, JAKB, OLAV, and OLA2 delimit areas

where the basement drops from about 300 m to 1,000 m depth.

3 Coda waves and coda Q methods

Coda wave of local earthquakes can be explained as backscattered S-waves from lateral heterogeneities distributed uniformly in the lithosphere (Aki 1969; Aki and Chouet 1975). The scattering is produced by irregular topography, complex surface geology, and heterogeneous elastic properties of the rocks, faults, and cracks, which are more frequent near the surface and less in deep region (Kumar et al. 2005). This implies that the decay of coda wave amplitudes as a function of lapse time (time measured from the origin time) are similar to each other for different earthquakes in a given area, independently of the source and receiver locations (Biswas and Aki 1984). The decay of coda wave amplitude with lapse time, according to Aki (1969), at a particular frequency, is only due to energy attenuation and geometrical spreading but independent of earthquake source, path propagation, and site amplification. The attenuation of seismic waves is the sum of intrinsic and scattering attenuation, where, in the first case, the energy is converted in heat through anelastic absorption and in the second case it is redistributed through refraction, reflection, and diffraction at random discontinuities present in a homogeneous medium (Kumar et al. 2005).

After the advent of coda wave theory by Aki and Chouet (1975) and Sato (1977), many studies (e.g., Herraiz and Espinosa 1987; Kumar et al. 2005; Kvamme and Havskov 1989; Rautian and Khalturin 1978) have shown that the coda Q factor increases with frequency through the relation

$$Q(f) = Q_0 \left(\frac{f}{f_0}\right)^{\eta} \tag{1}$$

where Q_0 is the quality factor in the reference frequency f_0, usually 1 Hz, and η is the frequency parameter, which is close to unity. These parameters vary according to the heterogeneities of the medium, seismicity, tectonics, and geological

features of each region (e.g., Jin and Aki 1988, 1989; Moncayo et al. 2004).

However, (Morozov 2008, 2009a, b) and Morozov et al. (2008) have questioned the frequency-dependence of coda Q quality factor (Q_c), as expressed by Eq. 1, and proposed a frequency-independent coda attenuation based on geometrical attenuation (γ) and effective attenuation (Q_e). In this work, these two approaches are tried and a description of both is given below.

3.1 The single scattering model

Assuming single scattering from randomly distributed heterogeneities Aki and Chouet (1975) showed that the coda waves amplitude at frequency f and elapsed time from the origin, t, can be expressed as:

$$A(f,t) = S(f)t^{-\nu}e^{-\frac{\pi f}{Q(f)}t} \tag{2}$$

where $S(f)$, is the source function at a frequency f, ν is the geometrical spreading parameter and $Q(f)$ the coda wave attenuation quality factor (Q_c), representing the attenuation of the medium. $S(f)$ is considered a constant as it is independent of time and radiation pattern. The parameter ν can assume the values 1.0 (for body wave scattering), 0.5 (for surface wave scattering), and 0.75 (for diffusive waves). As coda waves are mainly S to S backscattered waves (Aki 1981; Kvamme and Havskov 1989), the spreading parameter $\nu = 1$ is used in this study. However, as Aki and Chouet (1975) noted, the dependence of different envelopes on time are relatively insensitive to the value ν. For most frequencies the estimates of $Q(f)$ for $\nu = 0.5$, 0.75, or 1.0 in the Kanto region differ by less than 20%. For PGSZ these estimates are in the range observed by Aki and Chouet (1975) for frequencies up to about 10 Hz as will be discussed later.

Equation 2 is valid only if the coda window begins at least after twice the S wave propagation time, $2(T_s - T_o)$, to avoid the effects of direct S-wave in the coda window and to validate the assumption used in the model that receiver and source are very close (Rautian and Khalturin

1978). Or in other words, the scattering is not a function of the distance between receiver and source.

Taking the natural logarithm of Eq. 2, we obtain

$$\ln A(f, t) + v \ln(t) = \ln(S(f)) - \pi f t / Q(f)$$
$$\ln[A(f, t)t] = k - bt, \text{ for } v = 1 \qquad (3)$$

The above equation represents a straight line where $b = \pi f/Qc$ and $k = \ln S(f)$. Hence, Q_c can be obtained from the slope of the linear regression of $\ln[A(f, t)*t]$ versus t, for a constant frequency. Then, in order to determine Q_c, the seismogram is initially narrow-band-pass filtered at different central frequencies. Q_c is determined for each frequency band and lapse time window, as will be seen in Section 4. For this, the SEISAN package was used (Havskov and Ottomöller 2008).

3.2 The independent frequency model

Contrary to most studies of attenuation of seismic waves based on the decay of coda-wave amplitude, $Q_c(f)$, Morozov (2008, 2009a) presented a new approach to the subject, particularly with respect to the dependence of $Q(f)$ with frequency as expressed by Eq. 1. The main problem is related to the assumed theoretical models for the geometrical attenuation, as expressed by Eq. 2, which, according to Morozov (2009b), is insufficiently accurate to constrain the actual relationship between the geometrical spreading, anelastic dissipation, and scattering. The $Q_c(f)$ model uses a number of strong assumptions, such as the uniform velocity background, perfectly known geometrical spreading, absence of free-surface effects and lithospheric reflectivity, and isotropic and often uniformly distributed scattering (Morozov 2009b). This inaccuracy often leads to significant exaggeration of the attenuation effects, and particularly scattering.

To resolve this problem, Morozov (2008, 2009a) proposed a new approach using the temporal attenuation coefficient, $\chi(f)$ instead of $Q(f)$, given by the following equation: $\chi(f) = \gamma + \frac{\pi f}{Q_e}$, where γ, the geometrical attenuation, is the frequency-independent part of $\chi(f) = \chi(0)$ and Q_e is the frequency independent coda attenuation or effective attenuation.

Studies of coda-wave and other attenuation features suggest that $Q(f)$ typically depends linearly on f, with both the intercept $\chi(0) = \gamma$ and slope $\frac{d(\chi(f))}{df} = \pi Q_e^{-1}$ being sensitive to the physical properties of the subsurface. For $\eta \approx 1$, the seismic amplitude (where the source and receiver effect had been removed) $P(t, f) = G_0(t).e^{\frac{-\pi f t}{Q(f)}} = aG_0(t); a \neq a(f)$, which means that the amplitude decay is purely geometrical and there is no need to invoke Q_c factor. Morozov (2008) introduced γ as being a combination of geometrical spreading and scattering. Also, he introduced the crossover frequency $f_c = \frac{\gamma Q_e}{\pi}$, at which the contributions of the geometrical and effective attenuation factors are equal. From $\chi(f) = \gamma + \frac{\pi f}{Q_e}$, we found ($\gamma$, Q_e) and the transformation to (η, Q_0) is found from $\ln \frac{q}{\gamma} + (1 - \eta) \ln f \approx \ln \left(1 + \frac{f}{f_c}\right)$, where $q = \frac{\pi f_0^\eta}{Q_0} = $ cte. See Section 6.2.

4 Data selection and analysis

The choice of data for analysis was preceded by a careful selection of magnitudes, station locations, epicentral distances, outcrop geology at the stations, and event depths. The duration magnitudes range from 1.2 to 3.4, and epicentral distances range between 1 km (JAKB and PDRB stations) to 72 km (JUAB station). The two earthquake sequences (1998 and 2005) were monitored by two different seismic networks. In the first case, the stations were installed further from the source and the network had a larger aperture (about 80 km), with stations installed in igneous outcrops of the craton (JUAB and SJOB) and in the Parecis basin (Fig. 2). Both networks used broadband (Güralp CMG-40T, 30 s to 50 Hz) and short-period 3-component sensors (S3000EQ, 1.0 to 100 Hz); both sampled at 100 sps.

Data was grouped by different geotectonic environments as well as the ability to sample structures at depths, depending on the event focal depth and the thickness of the sedimentary package at the station, which is shown to be a determining factor in the coda Q values. In this sense, the events could be divided into three groups: group A (stations in the basin and events detected by the two networks); group B (stations in the

craton and events detected by 1998–2002 network); and group C (A + B). Additionally, group A was divided into two subgroups (A1 and A2), as indicated in Table 1.

The events of the 1998 sequence occurred with depths between 0 and 6 km, with the majority (70%) between 3 and 6 km. The event sequence of 2005 was shallower, the deepest reaching only 3 km depth. Hypocenters were determined with the hypocenter code (Lienert and Havskov 1995). For the 1998 sequence, we used a Vp/Vs ratio = 1.71 and obtained the following quality locations parameters: rms travel time residual <0.10 s; horizontal error (ERH) <2.0 km; vertical error (ERZ) <2.0 km. For the 2005 sequence, higher Vp/Vs ratio was determined (Vp/Vs = 1.78) and better locations were possible as the stations were closer than the 1998–2002 network. In this case the following quality locations parameters: ERH < 0.5 km, ERZ < 1.0 km, and rms residual <0.05 s. The difference in the Vp/Vs ratios is due to the different diameter of the seismic networks: the larger aperture of the 1998 network, with some stations located outside the Parecis basin, samples a deeper part of the upper crust, whereas the smaller 2005 network actually gives a Vp/Vs more representative of the shallow sedimentary layers of the Parecis basin. Therefore, the events of 1998 and 2005 seismic sequences should sample different volumes of the Parecis basin.

To test the sensitivity of coda waves to the thickness of the basin sedimentary package, we used subgroups A1 and A2: A1 composed by the six stations in the northern part of the abrupt transition in the basin depth (BAT, FJKB, FSJB, FBO2, FBON, and PDRB), and A2 composed by the six stations to the south of the transition (CMA, JAKB, OLA2, FANB, TAGL, and FPOR) as shown in Fig. 2 and Table 1.

The single scattering method can be resumed in five steps. An example of processing is shown in Fig. 3 for two different events, one recorded by station JUAB (craton) in 1999 with epicentral distance of 70 km (Fig. 3a), and the other by station OLA2 (basin) in 2005, located 8.5 km from the epicenter (Fig. 3b).

1. The traces are filtered using narrow band-pass, six-poles Butterworth filters, at central frequencies $F = 1.5, 3.0, 6.0, 9.0, 12.0,$ and 18.0 Hz, with bands of 1–2, 2–4, 4–8, 6–12, 8–16, and 12–24 Hz, respectively.
2. Measurement windows are defined, starting at twice the S-wave travel time (START = 2.0 in Fig. 3), with durations from 25 to 60 s, in steps of 5 s. Figure 3 shows the results for a

Table 1 Distribution of the station groups A (stations in the basin), B (stations in the craton), and C (A + B) and subgroups A1 (stations in the north of the basin) and A2 (stations in the south of the basin) according to station geology

Group	No. of events	Sequence	Station location	Epicentral range (km)	Stations (Fig. 2)	Location	$Q_0 \pm \sigma$	$\eta \pm \sigma$
A	47	1998/2005	Basin	1–20	FBO2, JAKB, FSJB, PDRB, OLA2, BAT, FJKB, FBON, CMA, TAGL, FANB and FPOR	Basin	98 ± 12	1.14 ± 0.08
B	39	1998	Craton	35–70	SJOB and JUAB	Craton	167 ± 46	1.03 ± 0.04
C	86	1998/2005	Basin and craton	1–70	all stations, A + B	Basin and craton	99 ± 19	1.17 ± 0.02
A1	47	1998/2005	Northern basin	1–20	BAT, FJKB, FSJB, FBO2, FBON and PDRB	Northern basin	103 ± 30	1.19 ± 0.14
A2	47	1998/2005	Southern basin	1–20	CMA, JAKB, OLA2, FANB, TAGL and FPOR	Southern basin	78 ± 23	1.17 ± 0.14

Last two columns show resulting Q_0, η, and corresponding standard deviation (σ) fitted for all window lengths, as shown in Fig. 7
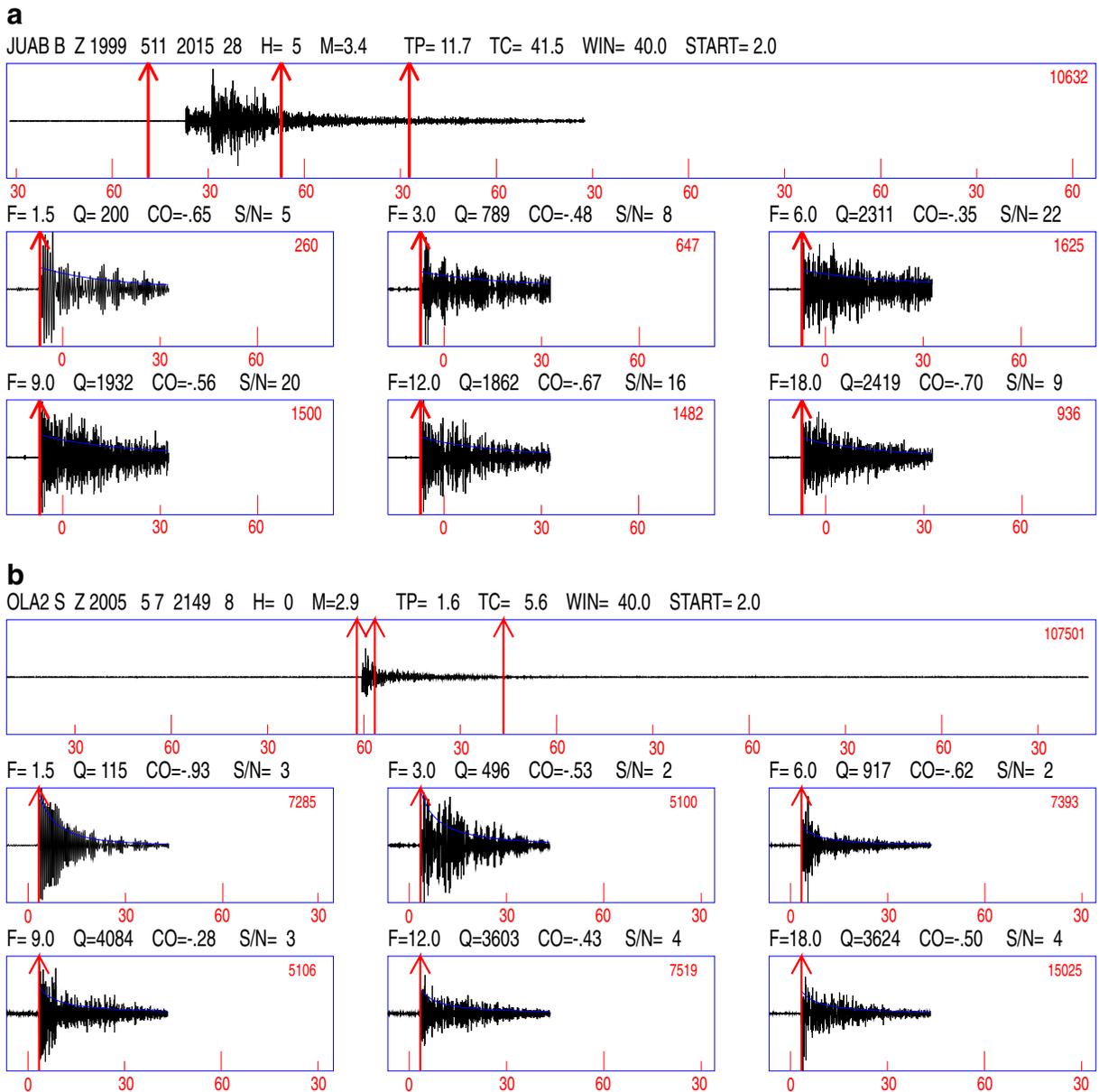
Fig. 3 Examples of unfiltered and band-pass-filtered traces for two events recorded at different epicentral distances and depths. The first recorded by station JUAB (**a**) in the craton (70 km distance) during the 1998–2002 sequence, and the second recorded by the close station OLA2 (**b**) in the basin (8.5 km distance) during 2005 seismic sequence. In each figure, the *top trace* is the original unfiltered signal where the *three vertical lines* indicate (*from the left*) origin time (T_o), window start ($2(T_s − T_o)$) and end of the coda window ($2(T_s − T_o)$ + WIN). On *top of first trace* is shown the station code and event identification. *Abbreviations*: *H* depth (km), *M* coda magnitude, *TP* P onset time, *TC* start of coda window (in seconds) from the origin, *WIN* window length, *START* start of coda window in terms of S travel time, always = $2(T_s − T_o)$, *F* central frequency in hertz, *CO* correlation coefficient, and *S/N* signal-to-noise ratio. The fitted envelope of each filtered segment is shown as a decay curve for each central frequency

Table 2 Average Q_c for each window length and central frequency

N	Window length	1.5 Hz (1–2) $Q_c \pm \sigma$	N	3.0 Hz (2–4) $Q_c \pm \sigma$	N	6.0 Hz (4–8) $Q_c \pm \sigma$	N	9.0 Hz (6–12) $Q_c \pm \sigma$	N	12.0 Hz (8–16) $Q_c \pm \sigma$	N	18.0 Hz (12–24) $Q_c \pm \sigma$	N
1	25	150 ± 56	18	205 ± 86	62	443 ± 202	41	650 ± 442	12	830 ± 673	3	2,263 ± 399	3
2	30	198 ± 72	16	229 ± 79	58	487 ± 242	33	769 ± 492	11	1,155 ± 798	4	2,422 ± 460	5
3	35	216 ± 76	20	251 ± 86	58	527 ± 284	27	1,132 ± 319	13	1,744 ± 932	11	2,713 ± 566	8
4	40	221 ± 72	31	249 ± 91	42	538 ± 253	17	1,384 ± 458	21	1,996 ± 820	22	3,423 ± 687	33
5	45	234 ± 84	30	251 ± 90	34	665 ± 346	23	1,494 ± 549	23	2,133 ± 692	32	3,269 ± 581	43
6	50	228 ± 74	24	254 ± 82	24	741 ± 323	17	1,601 ± 354	21	2,263 ± 356	27	3,367 ± 753	47
7	55	229 ± 71	22	263 ± 90	20	895 ± 366	17	1,601 ± 351	20	2,201 ± 294	24	3,119 ± 515	33
8	60	210 ± 55	21	248 ± 73	14	887 ± 334	15	1,566 ± 340	17	2,138 ± 283	20	2,979 ± 277	25

N is the number of Q_c values used for the average and σ is the standard deviation. Quality factor and standard deviation for the Parecis basin (group A): the functional formula $Q_c = Q_0 f^n$ for each window length is: (1) $(79 \pm 16) f^{(0.96 \pm 0.12)}$, (2) $(91 \pm 25) f^{(0.97 \pm 0.16)}$, (3) $(90 \pm 29) f^{(1.09 \pm 0.17)}$, (4) $(92 \pm 32) f^{(1.2 \pm 0.15)}$, (5) $(101 \pm 33) f^{(1.18 \pm 0.14)}$, (6) $(102 \pm 31) f^{(1.2 \pm 0.12)}$, (7) $(113 \pm 30) f^{(1.16 \pm 0.11)}$, (8) $(110 \pm 27) f^{(1.16 \pm 0.11)}$

window length (WIN) of 40 s. The signal-to-noise ratio (S/N) of each window and central frequency is determined by the ratio of the rms amplitude of the last 5 s of the window to the rms amplitude of 10 s of noise before the P-wave arrival. Windows with S/N less than 2 were discarded.

3. For each central frequency, the amplitude of the coda envelope ($A(f)$) is determined and the regression line of Eq. 3 is fitted. Q_c is determined from the regression coefficients. The amplitude decay corresponding to the calculated Q_c is shown in Fig. 3 with the blue lines. The correlation coefficient (CO) of this regression is used as a quality check of the Q_c. Only Q_c obtained with CO better than 0.45

are used. For the first event in Fig. 3a, Q_c for $F = 6$ Hz was not used (CO worse than 0.45). For the second event (Fig. 3b), frequencies of $F = 9$ and 12 did not have good enough correlation and were also discarded.

4. For each window length and central frequency, an average Q_c is determined with all earthquakes for all stations of the group (with S/N > 2 and CO better than 0.45).

5. For each window length Q_0 and η are determined with Eq. 1.

Different thresholds for the signal-to-noise ratio (S/N) and the correlation coefficient (CO) were tried. We chose S/N > 2 and CO > 0.45 because they represent a good compromise between

Table 3 Average Q_c for each window length and central frequency

N	Window length	1.5 Hz (1–2) $Q_c \pm \sigma$	N	3.0 Hz (2–4) $Q_c \pm \sigma$	N	6.0 Hz (4–8) $Q_c \pm \sigma$	N	9.0 Hz (6–12) $Q_c \pm \sigma$	N	12.0 Hz (8–16) $Q_c \pm \sigma$	N	18.0 Hz (12–24) $Q_c \pm \sigma$	N
1	25	145 ± 49	12	377 ± 73	11	769 ± 179	13	1,132 ± 162	20	1,528 ± 284	24	2,241 ± 342	33
2	30	145 ± 47	10	523 ± 67	6	841 ± 158	11	1,325 ± 244	23	1,629 ± 307	22	2,542 ± 400	33
3	35	155 ± 37	9	673 ± 91	5	979 ± 271	14	1,337 ± 273	17	1,830 ± 381	23	2,593 ± 416	28
4	40	177 ± 24	7	683 ± 85	3	1,101 ± 257	14	1,632 ± 360	21	1,959 ± 395	23	2,699 ± 465	28
5	45	199 ± 57	6	815 ± 143	2	1,240 ± 375	10	1,739 ± 421	18	2,127 ± 475	21	2,804 ± 542	28
6	50	228 ± 69	5	886 ± 0	1	1,349 ± 308	5	2,095 ± 450	13	2,428 ± 580	18	2,958 ± 457	22
7	55	225 ± 20	4	1,220 ± 0	1	1,343 ± 362	2	2,225 ± 687	7	2,692 ± 688	16	3,280 ± 610	23
8	60	240 ± 0	2	0 ± 0	0	1,527 ± 361	2	2,074 ± 622	5	2,990 ± 822	16	3,424 ± 644	21

N is the number of Q_c values used for the average and σ is the standard deviation. Quality factor and standard deviation for the Amazon craton (group B): the functional formula $Q_c = Q_0 f^n$ for each window length is: (1) $(105 \pm 9) f^{(1.07 \pm 0.04)}$, (2) $(113 \pm 21) f^{(1.09 \pm 0.07)}$, (3) $(133 \pm 34) f^{(1.05 \pm 0.1)}$, (4) $(158 \pm 41) f^{(1.02 \pm 0.1)}$, (5) $(183 \pm 52) f^{(0.98 \pm 0.11)}$, (6) $(205 \pm 68) f^{(0.97 \pm 0.12)}$, (7) $(203 \pm 76) f^{(1 \pm 0.13)}$, (8) $(220 \pm 105) f^{(0.99 \pm 0.15)}$

rejecting too much data and getting a reasonable number of events to calculate the average Q for each data group.

5 Results

Quality factors were estimated for three different datasets, each one representing a particular configuration of stations in relation to the seismic sources (Table 1 and Fig. 2). Datasets A and B sample two different areas: Parecis basin (dataset A) and craton (dataset B). The average Q_c for the whole region was obtained using dataset C (A + B). The results for the basin, craton, and the whole region are presented in Tables 2, 3, and 4, for the six central frequencies and eight lapse time windows.

To make a meaningful comparison of Q_c from different regions, according to Havskov et al. (1989), it is important to evaluate the maximum volume sampled by each data group. The attenuation of coda waves in the single scattering model, assuming a constant velocity and a constant density of scatters, is the average amplitude decay of back-scattered waves on the surface of ellipsoid volume having earthquake source and station as foci (Pulli 1984). The observed Q_c reflects the average attenuation properties of the volume of ellipsoid at an average depth, $h = h_{av} + d_2$, where h_{av} is the average focal depth of the events and $d_2 = \sqrt{(d_1)^2 - (d_{av})^2}$ is the small semi-axis of the

ellipsoid for d_{av} as average epicentral distance (Havskov et al. 1989; Mukhopadhyay et al. 2008; Pulli 1984). The large semi-axis of the ellipsoidal volume is $d_1 = vt/2$ for lapse time t and velocity v of the S-wave ($v = 3.5$ km/s). The average lapse time is taken as $t = ts + Wl/2$ where ts is the starting time of the coda window and Wl is the coda window length. Since we do not have a set of events detected by the same station, but instead a set of events detected by a set of stations, we used averages for each data set. For d_{av} (average epicentral distance), we used the distance between just one representative event, located in the middle of the seismogenic fault, labeled as a white star in Fig. 4, and the most distant stations from this source: JUAB, for group B; BAT, for subgroup A1; and FPOR, for subgroup A2 (see Fig. 4). For window length (Wl), we used the one that was most representative of each data group. For group B Wl = 45 s; for subgroups A1 and A2 Wl = 35 s. Then, we have the following average lapse time (t): for (JUAB, BAT, and FPOR) = (64.5, 22.6, and 22.6 s).

Figure 4 shows 2-D projections of the ellipsoidal regions sampled by coda waves for the group B and subgroups A1 and A2. The foci of the ellipses are formed by the event located in the middle of the seismogenic fault (star in the figure) and the stations JUAB, located in the craton (group B), BAT located in the northern basin (subgroup A1), where the sediments thickness are about 300 m, and FPOR (subgroup A2),

Table 4 Average Q_c for each window length and central frequency

N	Window length	1.5 Hz (1–2) $Q_c \pm \sigma$	N	3.0 Hz (2–4) $Q_c \pm \sigma$	N	6.0 Hz (4–8) $Q_c \pm \sigma$	N	9.0 Hz (6–12) $Q_c \pm \sigma$	N	12.0 Hz (8–16) $Q_c \pm \sigma$	N	18.0 Hz (12–24) $Q_c \pm \sigma$	N
1	25	148 ± 53	30	220 ± 99	73	493 ± 243	54	886 ± 567	32	1,397 ± 659	27	2,242 ± 341	36
2	30	173 ± 66	26	242 ± 94	64	544 ± 286	44	1,074 ± 634	34	1,532 ± 579	26	2,525 ± 404	38
3	35	192 ± 66	29	264 ± 103	63	626 ± 369	41	1,239 ± 324	30	1,802 ± 643	34	2,619 ± 443	36
4	40	211 ± 64	38	260 ± 105	45	699 ± 398	31	1,498 ± 453	42	1,977 ± 632	45	3,048 ± 673	61
5	45	227 ± 79	36	261 ± 104	36	773 ± 443	33	1,593 ± 536	41	2,130 ± 615	53	3,068 ± 616	71
6	50	228 ± 72	29	261 ± 93	25	825 ± 396	22	1,759 ± 448	34	2,326 ± 452	45	3,225 ± 677	69
7	55	228 ± 65	26	274 ± 106	21	928 ± 387	19	1,726 ± 463	27	2,374 ± 487	40	3,183 ± 558	56
8	60	213 ± 55	23	248 ± 73	14	933 ± 373	17	1,658 ± 417	22	2,448 ± 607	36	3,167 ± 489	46

N is the number of Q_c values used for the average and σ is the standard deviation. Quality factor and standard deviation for the region (group C). The functional formula $Q_c = Q_0 f^n$ for each window length is: (1) $(69 \pm 13) f^{(1.17\pm0.09)}$, (2) $(77 \pm 16) f^{(1.18\pm0.1)}$, (3) $(88 \pm 19) f^{(1.17\pm0.1)}$, (4) $(98 \pm 26) f^{(1.18\pm0.11)}$, (5) $(108 \pm 30) f^{(1.17\pm0.11)}$, (6) $(111 \pm 33) f^{(1.18\pm0.11)}$, (7) $(118 \pm 31) f^{(1.16\pm0.11)}$, (8) $(112 \pm 30) f^{(1.18\pm0.11)}$
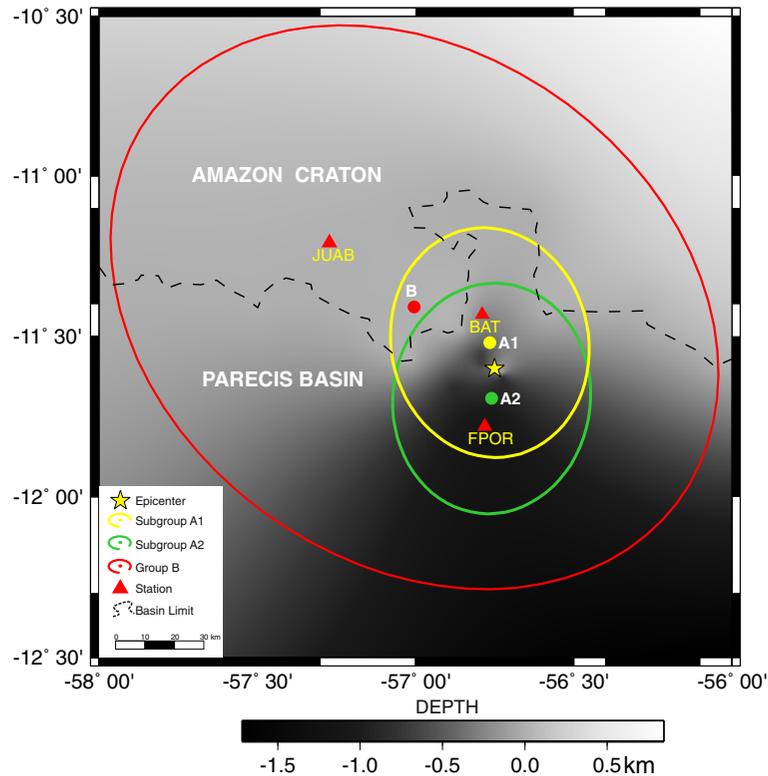
Fig. 4 2-D projections of the ellipsoidal volumes sampled by the coda waves of group B (*red ellipse*) and subgroups A1 and A2 (*yellow and green ellipses*, respectively). The *star* denotes a representative epicenter located in the middle of the seismogenic fault (one focus of the ellipse). The stations are indicated by *triangles* and they are the other focus of each ellipse. JUAB is located in the Amazon craton, BAT in the northern part of the Parecis basin,

where the basin depth is around 300 m and FPOR is located in the southern part of the basin, where the depth is around 1,500 m. The center of each ellipse is indicated by a *circle*. The ellipse for JUAB station samples half the basin and half the craton; the other two ellipses mainly sample the basin areas. The *dashed line* indicates the limit between the two tectonic areas

located in the southern part of the basin, where the sediments thickness are about 1,500 m.

Figure 5 shows the differences in the behavior of the coda waves for different windows lengths for the groups A, B, and C. Group B (stations in the craton) shows a trend of higher Q_0 compared to basin stations (groups A). The increase in Q_0 for group B should be related to large volume sampling of basement due to the deeper penetration of seismic waves in the lithosphere where the rocks are more homogeneous and consequently have lower attenuation (high Q_0). Considering the parameters of the maximum averaged ellipsoid volume sampled by each data group (Fig. 4), the penetration ($h = h_{av} + d_2$) of coda waves for group B is more than two and half larger than

for subgroups A1 and A2, 118 km against 42 km for both subgroups. This suggests that attenuation is stronger (lower Q) for the groups that sample predominantly basin areas. Figure 5 shows that the results for group A (stations in the basin) and group C (all stations in the basin and in the craton, A + B) are similar. This could be related with the fact that we have more data for coda wave calculation coming from stations located on the basin (see Tables 2, 3, and 4).

To further investigate the sensitivity of the coda waves to the depth of basement top in the Parecis basin (i.e., sediment thickness), we compared the results of subgroups A1 and A2: A1 sampling the shallower northern part of the basin, and A2 sampling predominantly the deeper southern part
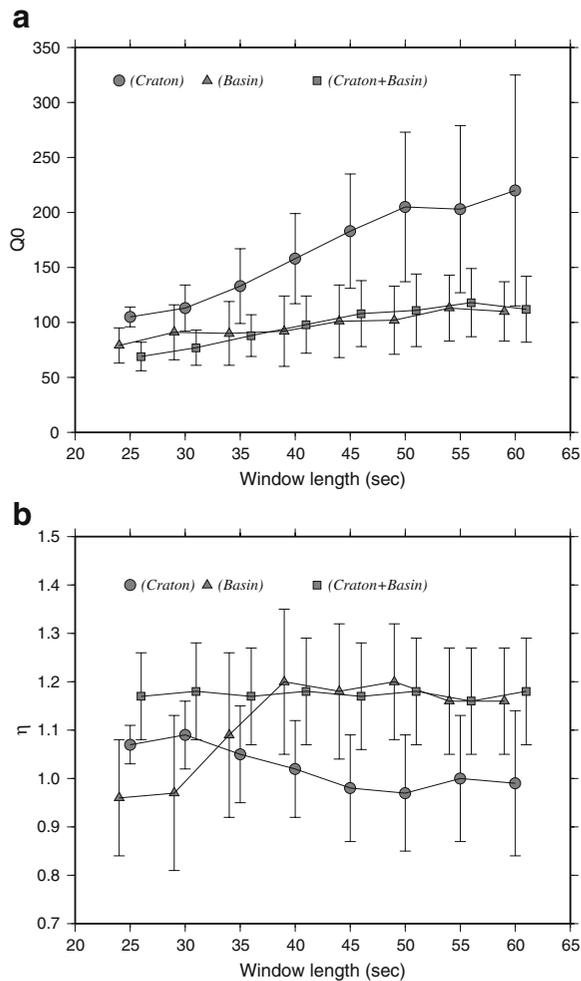
a

b

Fig. 5 Plots of Q_0 (**a**) and frequency parameter η (**b**) with window length for groups A (stations in the basin), B (stations in the craton), and C (stations in the basin and craton). *Symbols* for each window length were slightly shifted for the sake of clarity to avoid overlapping the *error bars*

a

b

Fig. 6 Plots of Q_0 (**a**) and frequency parameter η (**b**) with window length for sub-groups *A*1 (six stations in shallow, northern part of the basin) and *A*2 (six stations in southern, deeper part of the basin). *Symbols* for each window length were slightly shifted for the sake of clarity to avoid overlapping the *error bars*

of the basin. Subgroups A1 and A2 are on opposite sides of the abrupt change in basement depth (Fig. 2). Despite the large uncertainties, Fig. 6 confirms that the stations in the deeper part of the basin (A2) produce stronger attenuation (lower Q) compared with shallower basin (A1).

Figure 6 also shows that Q_0 increases with window length for subgroup A2 (stations in the deeper part of the basin) but do not depend on the window length for stations in shallower basin (A1). Given the uncertainties in Q_0 and η, we estimated the representative attenuation coefficients
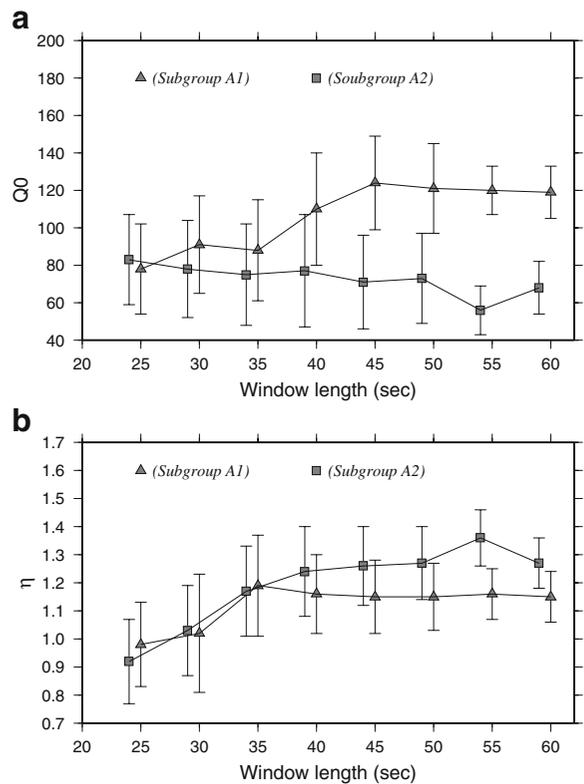
by taking the average of the Q_c measurements for all eight window lengths, as shown in Fig. 7. For each group the functional form $Q_c = Q_0 f^{\eta}$ was fitted using the average Q_c of the eight window lengths. The results for all groups are shown in Table 1.

6 Discussion

The estimates of the average quality factor for coda waves (Q_c) for the three groups (Fig. 7) are different, both with respect to the values of Q_0 and the frequency parameter η. This can be explained by the fact that each data group samples different volumes of the crust (see Fig. 4), due to the positions of stations in relation to the seismic source (hypocentral distance) as well as to their
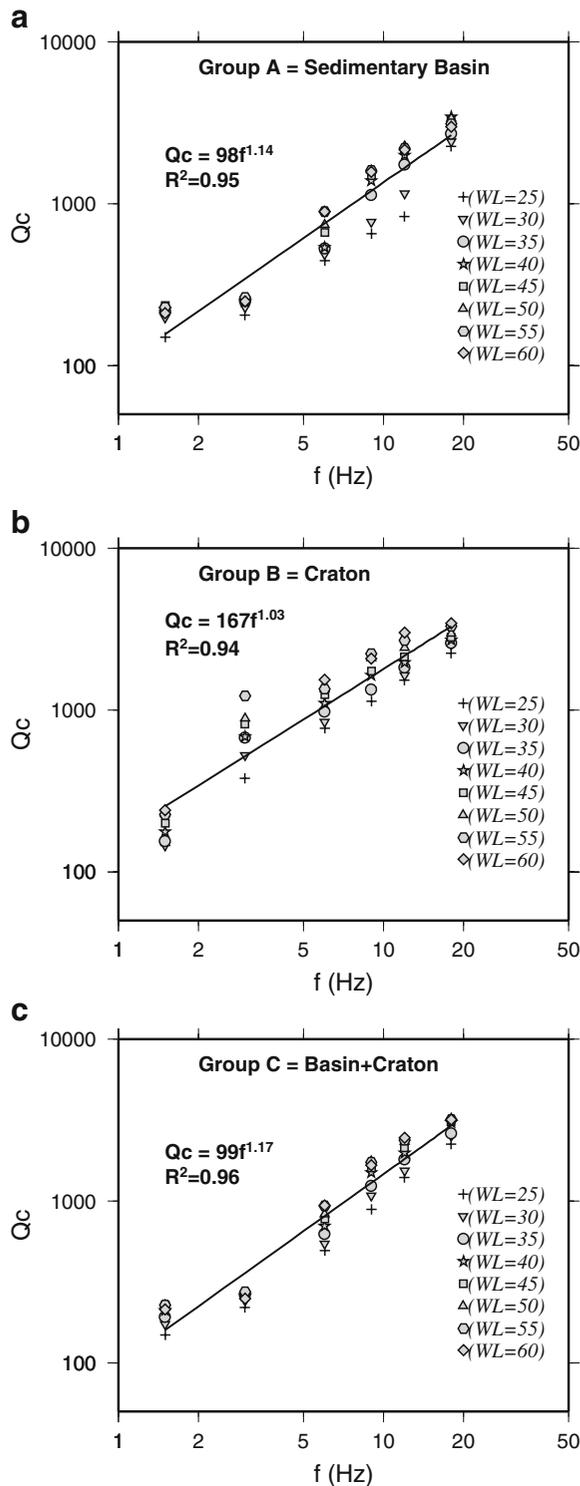
Fig. 7 $Q_c(f)$ for all data groups with fitted relationship $Q_c = Q_0 f^\eta$. Data points refer to the eight windows lengths (*WL*). **a** Group A (stations in the basin); **b** group B (stations in the cratonic basement), $Q_c = 167\ f^{1.03}$; and **c** group C (all stations of both networks), $Q_c = 99\ f^{1.17}$. R^2 is the correlation coefficient

geotectonic environment. Thus, the lateral and vertical heterogeneities sampled by each group are different, and affect, therefore, in different forms the coda wave energy decay.

The most significant difference shown by our results relates to the two main geotectonic environments sampled by the coda waves: Phanerozoic sediments of Parecis basin and the pre-Cambrian basement of the Amazon craton. Moreover, the sedimentary basin thickens rapidly from north to south (Figs. 2 and 4). Depending on the position of the seismic station, the coda waves sample more sedimentary or more basement rocks, two contrasting environments in terms of density, seismic velocities, and heterogeneities. All these factors affect differently the decay of the coda waves. In addition, stations more distant from the source sample deeper structures, and in this case sample predominantly the crystalline cratonic basement, where the rocks are denser, presumably more homogeneous and with higher seismic speed. This generally implies an increase in coda quality factor Q (lower attenuation) due mainly to a reduction in heterogeneities as observed by Pulli (1984) and Kvamme and Havskov (1989). The increase in Q_0 for group B ($Q_c = 167\ f^{1.01}$, more distant stations) could be explained by the decrease in heterogeneities with depth, as compared with the results for the basin area ($Q_c = 98\ f^{1.14}$, group A with closer stations; see Table 1).

The effect of the thickness of the sedimentary layer in the coda wave attenuation is more clear if we compare the Q_0 and the frequency parameter η from subgroups A1 (northern stations) and A2 (southern stations), as shown in Table 1 and Fig. 4. For the shallower, northern part of the basin $Q_c = 103 \pm 30\ f^{1.19 \pm 0.14}$ and for the deeper, southern part $Q_c = 78 \pm 23\ f^{1.17 \pm 0.14}$. Here should be taken in account that both subgroups sample the same crustal volume, as can be seen in Fig. 4. So, the attenuation differences between subgroups A1 and

A2 are due to differences in attenuation in the two uncommon areas shown in the ellipses projections of Fig. 4, the areas that do not overlap, since in the common area of ellipses projections the coda waves from both subgroups travel by the same region. However, in the uncommon areas the attenuation properties sampled by each subgroup are quite different. For the subgroup A1, in the upper area inside the yellow ellipse and outside the green ellipse, coda waves travel by cratonic areas and in the thinner part of the basin (<200 m thick) where the attenuation should be lower compared with the southern part of the basin, inside the green ellipse and outside the yellow where the sediments are about 1,500 m thick.

This shows that the energy of coda waves is attenuated more strongly in sedimentary areas where sediments are thicker compared to those where sediments are thinner . Thus, coda waves could be used to help characterize geological structures in subsurface as the coda Q is highly affected by the sedimentary layer thickness.

The differences between Q_c in sedimentary and basement environments are more pronounced in low frequencies, as it can be seen in Fig. 8 for the craton (group B) and the southern, thicker part of the Parecis basin (subgroup A2). The larger Q_0 (167) in the craton compared to the lower Q_0 (78) in the deep basin can be interpreted as due to a more homogeneous medium of the cratonic basement rocks.
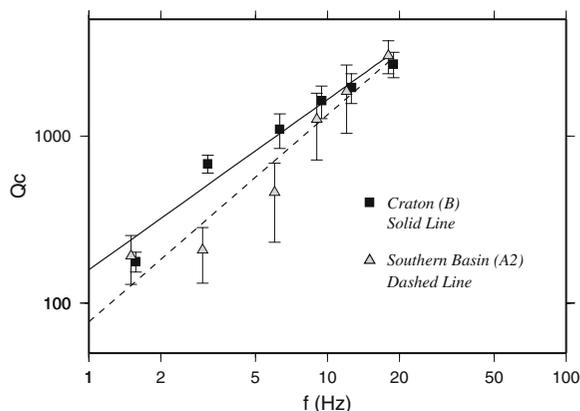

Fig. 8 Plot of $Q_c \times f$ (Hz) for craton stations (group B) and southern part of the Parecis basin (subgroup A2) for window length of 45 s

A comparison of frequency dependence of Q_c^{-1} observed in Baja California (Rebollar et al. 1985), Porto dos Gaúchos seismic zone (PGSZ, this study), Norway (Kvamme and Havskov 1989), and NE Brazil (Dias and Souza 2004) is shown in Fig. 9. The slopes of Q_c^{-1} vs. frequency curves for all tectonics regions are by and large in agreement, with Baja California, a very active seismic zone (Rebollar et al. 1985), presenting high attenuation in comparison with the three other similar stable zones. In the frequency of 6 Hz the attenuation in Baja California is about four times higher than in the other three stable areas and in all cases attenuation decreases with frequency.

6.1 Effect of the geometrical spreading parameter

Our study used the single scattering hypothesis with the value 1 for the geometrical spreading parameter (v), as it has been done by many others in the last three decades. However, Morozov (2008, 2009a) has questioned the common assumption of geometrical attenuation parameter $v = 1$ and the frequency dependence of Q_c. Rautian and Khalturin (1978) had observed that the values of Q_c varied only by about 20% if 0.5, 0.75, or 1.0 were used for the geometrical parameter. Aki and Chouet (1975) observed for the same frequency some variation in the parameter v among three different regions, and some variation with frequency in the same region. For Tsukuba region v increased from 0.7 (at 0.75 Hz) to 2.2 (at 12 Hz) and a clear frequency dependent Q was observed even allowing for variable geometrical parameter.

For the region of Porto dos Gaúchos, we tested the effect of different geometrical parameters for a window length of 45 s. We observed that increasing v from 0.5 to 1.5 doubles the values of Q_c at 12 Hz: from roughly 1,600 to 3,100 in the craton, and from 1,100 to 2,200 in the basin. Q_0 also doubles for the basin (from 70 to 160) but has little effect in the craton (changes from 200 to 160). Figure 10 shows Q_c for the craton and basin for two values of v. A change of the adopted geometrical spreading parameter in PGSZ generally affects $Q_c(f)$ for the basin and the craton in similar ways. Therefore, the difference in $Q_c(f)$ observed between groups sampling different geological structures is maintained.

Fig. 9 Comparison of Q_c^{-1} relationship obtained for Porto dos Gaúchos seismic zone (*PGSZ*) with other tectonic regions studied by others authors as indicated in the legend
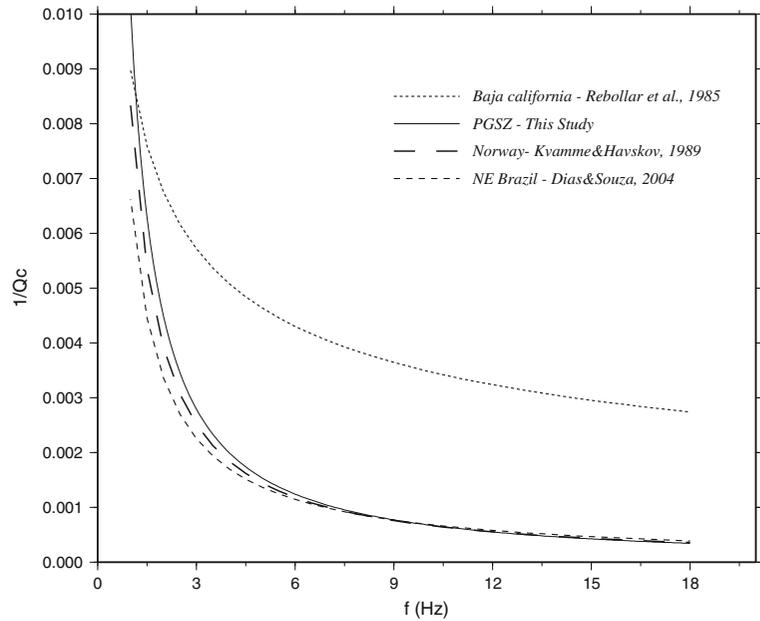
6.2 Coda Q: a new approach

Using Morozov (2008, 2009a) approach, we calculate the geometrical attenuation (γ), effective attenuation (Q_e^{-1}) and geometrical spreading parameters (ν) for the Porto dos Gaúchos seismic zone (Table 5).

From Fig. 11, we see that the cratonic zone sampled in this study is a zone of low attenuation with a crossover frequency of $f_c \approx 21$ Hz and it can be inferred that the geometrical attenuation dominates the coda amplitude decays, i.e., γ dominates that of Q_e even for $f = 18$ Hz. From the value $\gamma = 0.011$ s^{-1} and $Q_e = 5,882$,

Fig. 10 Dependence of Q_c with frequency for geometrical spreading parameter $\nu = 0.5$ and 1.5, for a window length of 45 s. *Solid lines* are the fitted functional for the craton (group B), and *dashed line* for the basin (group A)
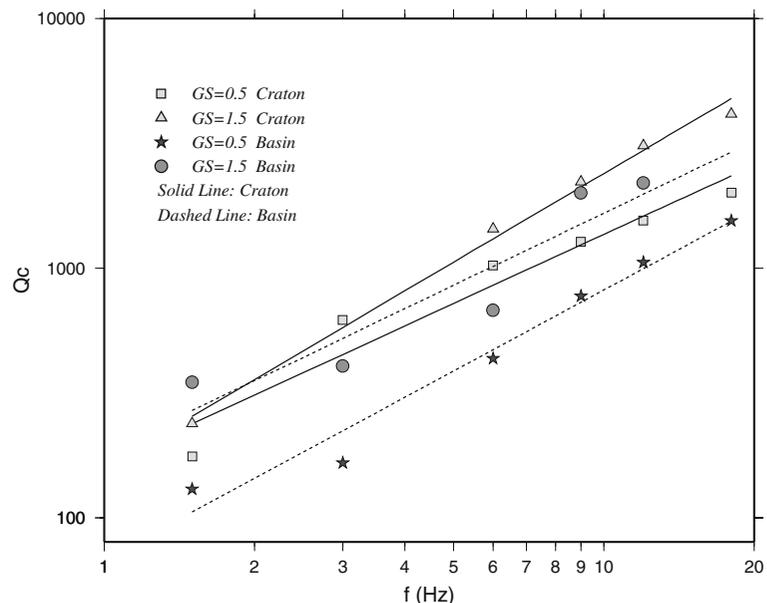
Table 5 Calculated parameters for the cratonic zone; where γ = geometrical attenuation, Q_e = effective attenuation, f_c = crossover frequency, ν = geometrical spreading parameter, Q_0 = frequency dependent quality factor at $f = 1$ Hz, η = frequency parameter, and WL = windows length

Values calculated using the independent frequency model approach (Morozov 2008) (η, Q_0) were obtained from (γ, Q_e) $\chi(f) = \gamma + \frac{\pi f}{Q_c} = \pi f/Q_c$							Values calculated from: $Q_c = Q_0 \left(\frac{f}{f_0}\right)^{\eta}$	
WL	γ	Q_e	f_c	ν	η	Q_0	Q_e/Q_0	Q_0	η
25	0.025	141,790	11,148	1.22	0.99	127	1,121	127	1.0
30	0.019	13,958	85.8	1.17	0.92	178	785	188	0.88
35	0.015	7,190	34.8	1.13	0.82	242	297	272	0.76
40	0.013	7,083	30.2	1.12	0.80	283	250	287	0.78
45	0.011	5,882	20.8	1.10	0.73	347	169	370	0.70
50	0.010	6,043	18.5	1.09	0.71	386	156	410	0.70
55	0.008	6,039	15.6	1.07	0.68	490	123	567	0.60
60	0.010	9,719	30.9	1.09	0.80	367	265	394	0.77

Fig. 11 Frequency dependence of Q_c^{-1} obtained for Parecis basin and Amazon craton for a lapse time of 45 s (**a**), and corresponding plot for the attenuation coefficient $\chi(f)$ according to Morozov's approach (**b**)
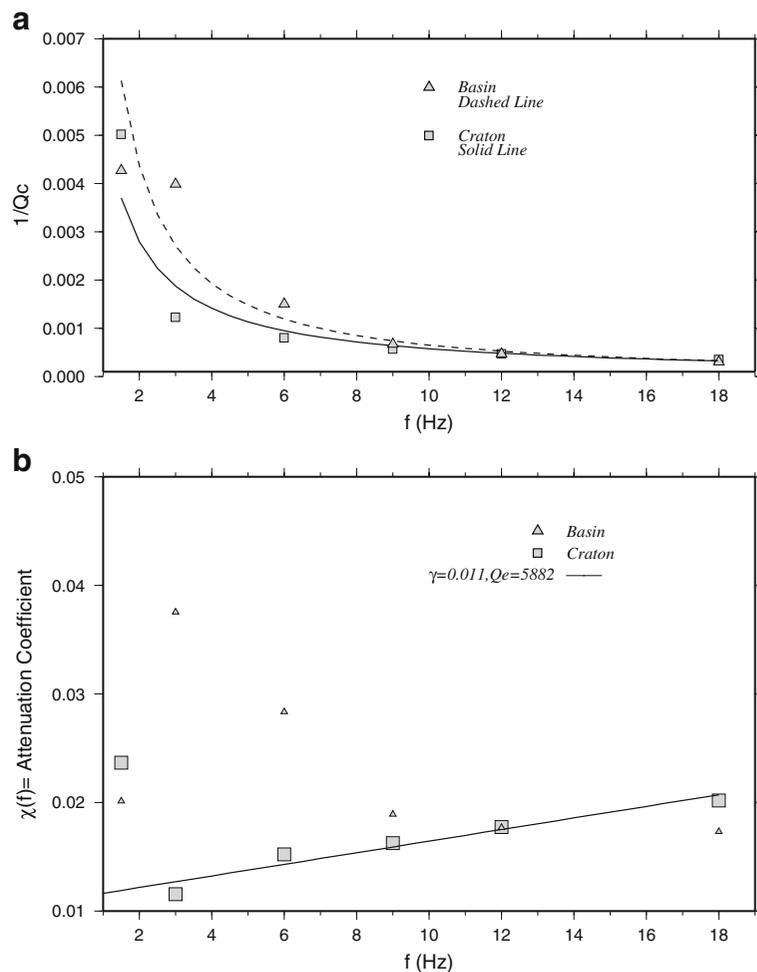
we infer a tectonically stable area associated with the craton. For the basin, the dominant effect may be reverberations (reflections) causing reduced amplitudes (increased $\chi(f)$) at 1 to 5 Hz.

Using the traditional calculation method (η, Q_0), we obtained $\eta > 1$ indicating a zone of low attenuation and high geometrical spreading. Another possibility is that one of our measurements carried out at lower frequency bias the results. It is seen from Fig. 11 that the data for the frequency 1.5 Hz is a possible outlier. Removing the 1.5 Hz data, we obtain $Q_c = 370 f^{0.7}$ for the cratonic area shown in Fig. 11 (see Table 5).

Using all the window lengths and fitting the data in the 3–18 Hz frequency band, we obtain for the cratonic data: (a) in the traditional way, $Q_c = 284 f^{0.79}$; (b) from the frequency-independent model, $\chi(f) = 0.014 + (\pi/8,928) f$, or $\gamma = 0.014$ s^{-1}, $Q_e = 8,928$ and $\nu \approx 1.12$. These values indicate low attenuation consistent with stable tectonic area.

Fitting the basin data using 3–18 Hz frequency band, we obtained: $\chi(f) = 0.04 - (\pi/2,582) f$ or $\gamma = 0.04$ s^{-1}; $Q_e = -2,582$; and $\nu \approx 1.35$. The value $\gamma = 0.04$ s^{-1} is typical of active tectonic zones and the variation of the geometrical spreading from $\nu \approx 1.0$ must be due to the reverberated waves in the sedimentary layer.

As we mentioned before, stations were installed in the Parecis basin; some of them on the thinner (subgroup A1) and others on the thicker (subgroup A2) part of the basin. The data for A1 in the 3–18 frequency band gave us an attenuation coefficient with $\gamma = 0.031$ s^{-1}; $Q_e = -3215$; $\nu \approx 1.27$; and for A2 $\gamma = 0.047$ s^{-1}; $Q_e = -2025$; $\nu \approx 1.42$. From these values, we infer that the southern part of the Parecis basin had larger γ than the northern part where the basement is shallow.

Using the obtained data for the region (Group C) with 3–18 Hz frequency band, we obtained: $\chi(f) = 0.035 - (\pi/2,941) f$ or $\gamma = 0.035$ s^{-1}, $Q_e = -2,941$, and $\nu \approx 1.31$. These values indicate a tectonic Porto Gaúchos active zone and also that most of the data are coming from stations located in the basin.

The negative values for Q_e obtained for the basin may be a problem, because they tell us that high-frequency amplitude somehow increases with propagation time. These results probably indicate that the model of Morozov does not allow determination of Q with enough resolution for areas with very high attenuation (very low Q) as in our case, and will deserve more attention in the future. It also should be mentioned that the values of about 0.035–0.04 s^{-1} for the tectonically active area, and the $\sim$0.01 s^{-1} within the Amazon craton are consistent with the results found by Morozov (2008) and Morozov et al. (2008). However, it would also be important to mention that the threshold separating active from stable areas, which Morozov et al. (2008) placed at =0.008 s^{-1}, could be higher in South America.

We propose that the increase of the γ factor for the basin zone is due to the velocity structure of the upper crust, where the thick sediments have a strong influence in the average attenuation, as opposed to the more homogeneous high-velocity layer of the cratonic area.

7 Conclusion

Applying the $Q_c(f)$ model, the observed differences in the values of $Q(f)$ are associated with the different tectonic-sedimentary environment, according to ellipsoid volumes sampled by each data group. The sensitivity of coda waves to the thickness of the sedimentary basin is clear. The estimated $Q(f)$ for the two cases clearly show that: for subgroup A1 (northern shallow basin, 100–300 m thick) $Q_c = 103 f^{1.19}$; for subgroup A2 (southern deeper basin, 300–1,500 m thick), $Q_c = 78 f^{1.17}$. The same set of events was used and the average lapse times where Q_c was measured are more or less the same in both cases. This ensures that the differences in Q_c must be related to the different geological structures sampled by each data group, mostly due to the different values of γ and ν in these areas. From the results shown above, we found that the f model (Morozov 2008, 2009a; Morozov et al. 2008), using a different concept of attenuation in a heterogeneous structure, with scattering likely occurring in the near-surface as opposed to random scattering at great depths in a uniform and isotropic background) explains the same data as the traditional $Q_c(f)$ model. We thus recommend that the f model should be tested with data sets in other areas.

From the f model applied to Porto Gaúchos earthquake data, Brazil, an important conclusion is that γ = geometrical attenuation is higher in intraplate active area of the Parecis basin than in the more stable area of the Amazon craton, consistent with similar studies in other regions (Morozov 2008, 2009a; Morozov et al. 2008).

So, we conclude that determination of coda Q with local earthquakes, besides giving information on seismic wave attenuation, can be used as additional qualitative information on the shallow crustal structure. Higher or lower values of Q_0 may indicate shallower or deeper basement depth.

References

Aki K (1969) Analysis of seismic coda of local earthquakes as scattered waves. J Geophys Res 74:615–631

Aki K (1981) Source and scattering effects on the spectra of small local earthquakes. Bull Seismol Soc Am 71:1687–1700

Aki K, Chouet B (1975) Origin of the coda waves: source, attenuation and scattering effects. J Geophys Res 80:3322–3342

Bahia RBC, Martins-Neto MA, Barbosa MAC, Pedreira AJ (2007) Análise da evolução tectonossedimentar da Bacia dos Parecis através de métodos potenciais. Revista Brasileira de Geociências 37(4):639–649

Barros LV, Assumpção M (2009) Basement depths in the Parecis basin (Amazon), with receiver functions from small local earthquakes in Porto dos Gaúchos seismic zone. Submitted to Journal to South American Earth Science

Barros LV, Assumpção M, Quintero R, Caixeta D (2009) The intraplate Porto dos Gaúchos Seismic Zone in the Amazon craton—Brasil. Tectonophysics 469:37–47

Biswas NN, Aki K (1984) Characteristics of coda waves: central and south-central Alaska. Bull Seism Soc Am 74(No. 2):493–507

Carvalho LA, Souza JL (2006) Attenuation of seismic coda waves in João Câmara (Rio Grande do Norte).

Acta Geodaetica et Geophysica Hungarica 41(1):133–142

Dias AP, Souza JL (2004) Estimates of coda Q attenuation in João Câmara area (Northeastern Brazil). Journal of Seismology 8:235–246

Gupta SC, Singh VN, Kumar AI (1995) Attenuation of coda waves in the Garhwal Himalaya, India. Phys Earth Planet Inter 87:247–253

Havskov J, Ottomöller L (2008) SEISAN: the earthquake analysis software for windows, solares, linux and macosx, version 8.2.1. Institute of Solid Earth Science, University of Bergen, Norway

Havskov J, Malone S, McClurg D, Crosson R (1989) Coda Q for the state of Washington. Bull Seismol Soc Am 79(4):1024–1038

Herraiz M, Espinosa AF (1987) Coda waves: a review. PAGEOPH 125(4):499–577

Herrmann R (1980) Q estimates using the coda of local earthquakes. Bull Seismol Am 70(2):447–468

Ibáñez JM, Del Pezzo E, Del Miguel F, Herraiz M, Alguacil G, Morales J (1990) Depth-dependent seismic attenuation in Granada zone (Southern Spain). Bull Seismol Soc Am 80(5):1232–1244

Jin A, Aki K (1988) Spatial and temporal correlation between coda Q and seismicity in China. Bull Seismol Soc Am 78:741–769

Jin A, Aki K (1989) Spatial and temporal correlation between coda Q^{-1} and seismicity and its physical mechanism. J Geophys Res 94:14041–14059

Johnston AC (1989) The seismicity of stable continental interiors. In: Gregersen S, Basham PW (ed) Earthquakes at North Atlantic passive margins: neotectonics and post-glacial rebound. Kluwer Academic Publishers, Kluwer, pp 299–327

Kumar N, Parvez IA, Virk HS (2005) Estimation of coda wave attenuation for NW Himalayan region using local earthquakes. Phys Earth Planet Inter 151:243–258

Kvamme LB, Havskov J (1989) Q in Southern Norway. Bull Seismol Soc Am 75(5):1575–1588

Leite JA, Saes GS (2003) Geocronologia Pb/Pb de zircões detríticos e análise estratigráfica das coberturas sedimentares Proterozóicas do sudeste do Cráton Amazônico. Rev do Instituto de Geociências da USP, São Paulo 3:113–127

Lienert BR, Havskov J (1995) A computer program for locating earthquakes both locally and globally. Seism Res Lett 66(5):26–36

Mendiguren JA, Richter FM (1978) On the origin of compressional intraplate stresses in South America. Phys of the Earth and Planet Int 16:318–326

Morozov IB (2008) Geometrical attenuation, frequency dependence of Q, and the absorption band problem. Geophys J Int 175:239–252

Morozov IB (2009a) Thirty years of confusion around "scattering Q? Seismol Res Lett 80:5–7

Morozov IB (2009b) Temporal variations of coda Q: an attenuation-coefficient view. http://seisweb.usask.ca/ibm/papers/Q/. Accessed 12/15/2009

Morozov IB, Zang C, Duenow JN, Morozova EA, Smithson SB (2008) Frequency dependence of coda Q, part I: numerical modeling and examples from peaceful nuclear explosions. Bull Seis Am 98(6):2615–2628

Moncayo E, Vargas C, Durán J (2004) Temporal variation of coda-Q at Galeras Volcano, Colombia. Earth Sci Res J 8(1):19–24

Mukhopadhyay S, Sharma J, Massey R, Kayal JR (2008) Lapse-time dependence of coda Q in the source region of the 1999 Chamoli earthquake. Bull Seism Am 98(4):2880–2086

Nuttli OW (1973) Seismic wave attenuation and magnitude relations for eastern North America. J Geophys Res 78:876–885

Pulli JJ (1984) Attenuation of coda waves in New England. Bull Seism Am 74(4):1149–1166

Rautian TG, Khalturin VI (1978) The use of the coda for determination of the earthquake spectrum. Bull Seism Soc Am 68:923–948

Rebollar CJ, Traslosheros C, Alvarez R (1985) Estimates of seismic waves attenuation in northern Baja California. Bull Soc Seismol 75(5):1371–1382

Sato H (1977) Energy propagation including scattering effects, single isotropic scattering approximation. J Phys Earth 25:27–41

Sharma B, Teotia SS, Kumar D (2007) Attenuation of P, S, and coda waves in Koyna region, India. J Seismology. doi:10.1007/s10950-007-9057-z

Singh S, Herrmann R (1983) Regionalization of crustal coda Q in the continental United States. J Geophys Res 88(No. B1):527–538

Souza JL, Mitchell BJ (1998) Lg coda Q variations across South America and their relations to crustal evolution. Pure Appl Geophys 153:587–612

Tassinari CCG, Bittencourt JS, Geraldes MC, Macambira MJB, Lafon JM (2000) The Amazonian Craton. In: Cordani et al (ed) Tectonic evolution of South America, 31st Int Geol Congr Rio de Janeiro, pp 41–95